Delocalized Lattice Plasmon Resonances Show Dispersive Quality Factors

Wei Zhou,[†] Yi Hua,[†] Mark D. Huntington,[†] and Teri W. Odom*,[†,‡]

[†]Department of Materials Science and Engineering, Northwestern University, 2220 Campus Drive, Evanston, Illinois 60208, United States

[‡]Department of Chemistry, Northwestern University, 2145 Sheridan Road, Evanston, Illinois 60208, United States

ABSTRACT: This Letter describes how out-of-plane lattice plasmon (OLP) resonances in 2D Au nanoparticle (NP) arrays show dispersive quality factors. These quality factors can be tailored simply by controlling NP height. Numerical calculations of near-field optical properties and band diagrams were performed to understand the measured dispersion effects of the OLPs. The results revealed that delocalized OLPs are a type of surface Bloch mode composed of many Bloch harmonics. As the OLP dispersion evolves from a stationary state to a propagating state, the nonradiative loss decreases because of weak local field confinement, whereas the radiative loss increases because of strong coupling to the leaky zero-order harmonic.

SECTION: Plasmonics, Optical Materials, and Hard Matter
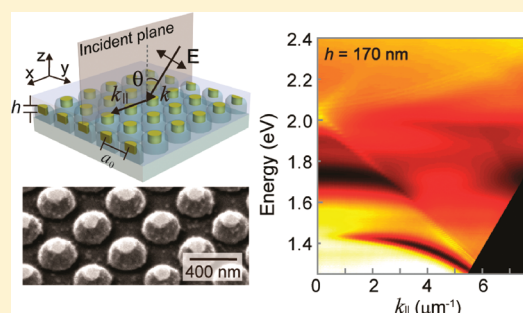
Surface plasmon resonances supported in metal nanostructures can concentrate optical fields into nanoscale volumes,[1,2] which is important for applications such as plasmonic nanolasers,[3,4] optical modulators,[5] chemical-biological sensors,[6] and nonlinear optical devices.[7,8] A slower depletion of plasmon energy is desirable to enhance local optical fields further and to achieve a narrow plasmon resonance line width.[9] The damping of plasmons is characterized by the resonance quality factor Q_{tot} (= $\lambda/\delta\lambda$ = $\omega/\delta\omega$), which is determined by both radiative (e.g., the electric-dipole radiation) and nonradiative (e.g., electron–electron, electron–phonon, and electron-defect interactions) processes.[10] For localized surface plasmon (LSP) resonances under the quasistatic condition (when the physical size of the resonator is small compared with local variations in the electromagnetic (EM) field), the nonradiative quality factor Q_{nr} has a theoretical upper limit of $(d\varepsilon'_m/d\omega)\omega/2\varepsilon''_m$ (<20 for Au in the optical range) because a major portion of the EM energy is stored and dissipated in the metal.[11] Recent work has shown that plasmonic structures with broken symmetries support multipolar dark LSP resonances beyond the quasistatic limit,[12–14] where both radiative and nonradiative losses are suppressed. These dark plasmon resonances cannot be easily tuned, however, without changing the overall geometry of the nanostructures.

Another strategy to achieve resonances with high Q_{tot} is to take advantage of lattice plasmon resonances in periodic nanoparticle (NP) arrays,[15–19] where the radiative loss is significantly reduced by dipolar interactions between NPs. In addition, because lattice plasmons are a type of delocalized plasmon resonance, Q_{nr} is not restricted to a theoretical upper limit for quasistatic LSPs. Because of challenges in fabricating NPs with heights (h) > 100 nm, most work has focused on in-plane lattice plasmons that are mediated by strong coupling between the in-plane dipole moments of the NPs.[15–19] The properties of in-plane lattice plasmons are typically described using the coupled dipole approximation (CDA) method;[15,16] however, because CDA uses plane-wave excitation to determine the fields self-consistently, there are challenges in characterizing dark plasmons, which cannot be excited by free-space light. Recently, we reported a new type of lattice plasmon in 2D arrays of large NPs (>100 nm in all three dimensions) that is mediated by out-of-plane dipolar interactions.[20] Out-of-plane lattice plasmons (OLPs) can be easily tuned by changing the height of the NPs in the array. Significantly, unlike in-plane lattice plasmons,[19] OLPs can maintain a high resonance quality factor Q_{tot} (>100) even when the dispersion relation is flat-banded.[20]

This Letter demonstrates that the Q_{tot} of OLPs is highly dispersive and depends sensitively on the height of the NPs. Computational methods reveal that OLPs can be considered as a type of surface Bloch mode composed of many Bloch harmonics. As the OLP dispersion evolves from a stationary state to a propagating state, the nonradiative loss decreases because a smaller portion of optical energy is stored in the NPs; in contrast, the radiative loss increases because more efficient coupling occurs between higher order Bloch harmonics and the leaky zero-order harmonic. This system provides a framework for understanding the dispersive properties of delocalized plasmon resonances supported by other types of plasmonic nanostructures.

Large areas (>1 cm^2) of 2D square arrays of Au NPs (periodicity $a_0 = 400$ nm, diameter $d = 160$ nm) were fabricated using soft nanolithography and template stripping.[20] To investigate the dependence of the OLP dispersion properties on NP height, we created a range of samples with different heights ($h = 90, 110, 135, 170$ nm). Zero-order reflection and transmittance spectra were measured under incident angles $\theta = 10$ to $60°$ using a home-built rotational stage, the in-plane wavevector $k_\parallel$ along the x direction (Figure 1A). We
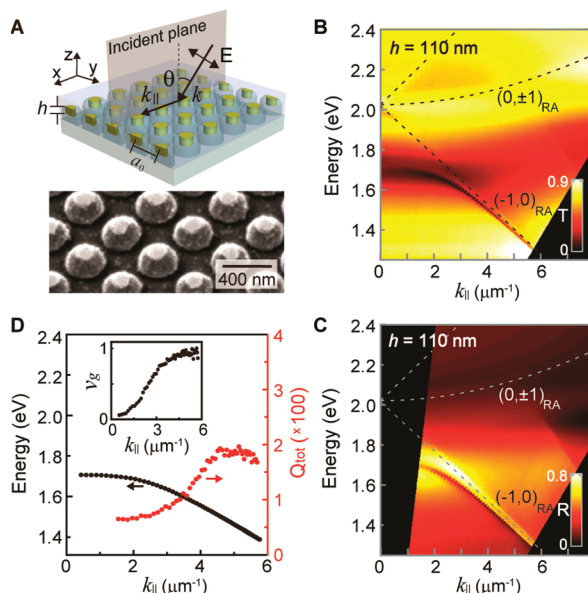
Figure 1. Out-of-plane lattice plasmons in 2D Au NPs exhibit wavevector-dependent resonance energies and quality factors. (A) Light excitation scheme under TM-polarized light and SEM image of Au NP arrays supported in PU at a tilted angle. (B) Measured transmittance (θ from 0 to 60°) and (C) reflectance (from 10 to 60°) spectra as a function of in-plane wavevector ($k_\parallel = k_0 \cdot \sin \theta$) and energy ($E = \hbar\omega$) for 2D Au NP arrays ($h = 110$ nm, $d = 160$ nm). (D) Measured resonance energy E and quality factor Q_{tot} of the out-of-plane lattice plasmons as a function of in-plane wavevector $k_\parallel$. (inset) Group velocity ν_g normalized to the speed of light in the dielectric environment surrounding the NP arrays ($n = 1.52$) as a function of $k_\parallel$.

illuminated the samples by collimated TM-polarized (p-polarized) white light from a halogen lamp (100 W) with a spot size of 2 mm. The reflected or transmitted light was coupled to a bundled optical fiber connected to a CCD spectrometer (Triax 552/LN$_2$–Cooled CCD, Horiba Jobin Yvon). All optical measurements were performed in index-matched conditions, where PU substrate ($n_{PU} = 1.55$) was in contact with an oil superstrate ($n_{oil} = 1.525$).

Figure 1B,C displays the measured transmittance and reflectance spectra as a function of in-plane wavevector ($k_\parallel = k_0 * \sin \theta$) and energy ($E = \hbar\omega$) for a Au NP array with $h = 110$ nm. Two types of resonances with different dispersion properties were observed: (1) a broad, in-plane plasmon resonance ($Q_{tot} \approx 8$) centered at $E = 1.7$ eV, which can be attributed to individual NPs;[20] and (2) a narrow, dispersive OLP resonance, which is flat-banded at small $k_\parallel$ and converges with the $(-1,0)$ Rayleigh anomaly (RA) at large $k_\parallel$. At small $k_\parallel$, the OLP exhibits a low normalized group velocity $[\nu_g/(c/n) = (\delta\omega/\delta k_\parallel)/(c/n)]$ (Figure 1D, inset) characteristic of a strong concentration of optical fields by plasmonic structures.[19,21] As $k_\parallel$ increases from 0 to 6 μm^{-1}, $\nu_g/(c/n)$ gradually increases

from 0 to 1 as the stationary state becomes a propagating one (Figure 1D, inset). The Q_{tot} of the OLPs can be determined by measuring the resonance linewidths in the reflectance and transmittance spectra; this value gradually increases from ~60 at $k_\parallel = 1.5$ μm^{-1} to ~180 at $k_\parallel = 5$ μm^{-1} (Figure 1D). This strong dependence of Q_{tot} on wavevector $k_\parallel$ indicates that the depletion time of stored plasmon energy is related to the dispersion properties of OLPs.

To understand the observed dispersion effects on the OLP resonances, we performed 3D finite-difference time-domain (FDTD) calculations to obtain the band diagrams and near-field optical properties of 2D periodic Au NP arrays.[22−25] One unit cell was modeled using a uniform mesh size of 3 nm (x, y, and z directions) with Bloch boundary conditions in the x-y dimensions and a perfectly matched layer in z. We used a pulsed, point-dipole source, which can generate optical fields with a broad range of frequency and wavevectors in the near-field, to excite OLPs across the entire k range, even when they cannot be excited by free-space light.[26] The dielectric constants of Au were included in the modeling by using a Lorentz-Drude model with parameters fitted to experimental data from 400 to 1000 nm,[27] and Au NP is modeled in a uniform dielectric environment ($n = 1.525$).

Figure 2A shows the FDTD-calculated band diagram of a 2D array of Au NPs ($h = 110$ nm), which displays the $E−k$
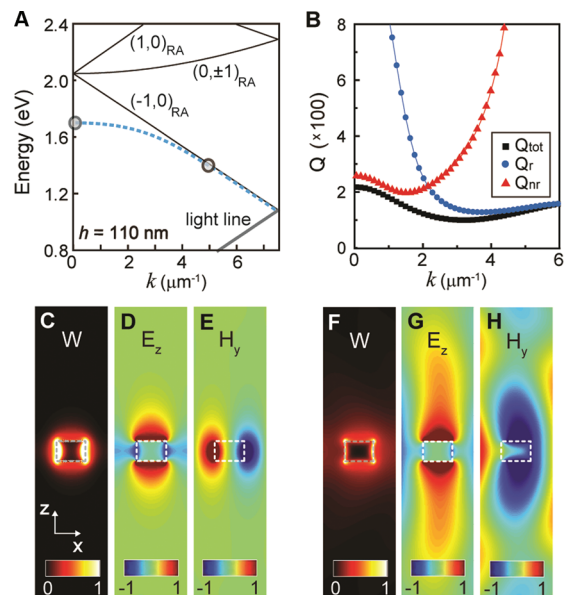
Figure 2. Optical energy of the out-of-plane lattice plasmon mode is concentrated in the Au NPs when the mode is a stationary state. (A) FDTD-calculated band diagram of 2D Au NP arrays ($h = 110$ nm). (B) FDTD-calculated quality factors Q_{tot}, Q_r, and Q_{nr} of OLP mode as a function of k. (C−H) FDTD-calculated maps of energy density, E_z and H_y at (C−E) a stationary state ($k = 0$), and (F−H) a propagating state ($k = 5$ μm^{-1}).

dispersion relations of various Bloch modes in the periodic structure. In addition to RAs associated with the different surface diffraction orders inherent in the 2D grating, the calculated band diagram contains a flat-banded dispersion curve above the light line that matches the one associated with the OLP mode in experiment (Figure 1D). Hence, the experimentally measured OLP resonances are a type of surface Bloch mode intrinsic to 2D periodic arrays of Au NP. These

1382

dx.doi.org/10.1021/jz300318v | J. Phys. Chem. Lett. 2012, 3, 1381−1385

modes do not rely on coupling between a localized and delocalized mode; therefore, OLPs can maintain a narrow resonance line width even when their dispersion is flat-banded with no overlap with that of a diffraction mode. As a type of Bloch mode, lattice plasmons can be decomposed into Bloch harmonics:[24,28] $E_k(x, y, z) = \Sigma_m U_k^m(y, z)e^{i((2\pi m)/(a_0)+k)x}$, where k is the fundamental wavevector along x in the first Brillion zone, a_0 is the period, m is the index of the Bloch harmonic, and $U_k^m(y, z)$ is the complex amplitude of each Bloch harmonic. On the basis of its dispersion relation (Figure 2A), the zero-order harmonic of the OLP mode lies above the light line (|$(2\pi m)/(a_0) + k$| < $n(\omega)/(c)$, $m = 0$) and can radiate energy into free space as photons, whereas other higher order harmonics are below the light line (|$(2\pi m)/(a_0) + k$| > $n(\omega)/(c)$, $m = \pm1, \pm2$, ...) and are evanescent modes bound to the plane of the NP arrays. Therefore, OLPs are a type of leaky surface Bloch mode. By reciprocity, OLPs can be excited by free-space light at oblique angles when the in-plane wavevector $k_{\parallel}$ of incident light matches with the wavevector k of the OLPs.

Compared with leaky Bloch modes in photonic crystal slabs where stored energy is dissipated only radiatively,[22,23] the OLP modes also involve nonradiative loss because of its plasmonic nature. Therefore, to understand the dispersion in Q_{tot}, we need to investigate the radiative quality factor Q_r and nonradiative quality factor Q_{nr} separately. From FDTD calculations, Q_r can be determined by the line width of resonant spectra in "lossless" Au NP arrays, where the dielectric constants of Au are modified by setting the imaginary part of the permittivity to zero.[29] Q_{nr} can then be calculated from the relation $Q_{tot}^{-1} = Q_r^{-1} + Q_{nr}^{-1}$. Figure 2B shows that the calculated Q_{tot} decreases from ~210 to ~100 as k increases from 0 to 3 μm^{-1} and then increases to 150 as k increases to 6 μm^{-1}, which is in qualitative agreement with the measured results (Figure 1D). After decomposing Q_{tot} into Q_r and Q_{nr}, we observed that each quality factor evolves very differently with k. At small k (<1 μm^{-1}), the radiative loss is extremely small, and the nonradiative loss dominates the total loss. As k increases from 0 to 2 μm^{-1}, Q_r drastically drops from >1000 to ~200, whereas the change of Q_{nr} is small. As k further increases from 2 to 6 μm^{-1}, Q_{nr} increases dramatically from ~200 to >1000, whereas the change of Q_r is small.

A microscopic near-field optical picture is needed to understand the dispersion effects on Q_{tot}. Figure 2C−H compares near-field optical properties as the dispersion evolves from a stationary state ($k = 0$) to a propagating state ($k = 5$ μm^{-1}). At the stationary state (Figure 2C), the EM energy density W ($W = (1/2)[Re[(d(\omega\varepsilon))/(d\omega)]|E|^2 + \mu|H|^2]$) map shows that a significant portion of the optical energy of OLPs is stored inside the Au NPs, which results in a dominant Q_{nr}. E_z shows maxima with the same phase on the top and bottom of the NPs, which corresponds to an out-of-plane dipolar oscillation (Figure 2D) with an extremely small radiation in z. H_y shows maxima with opposite phase on lateral edges of the NPs in x−z cross-section, which indicates that a circulating magnetic field around the NPs is coupled to the alternating charge current driven by E_z along the z axis (Figure 2E).

At the propagating state (Figure 2F), most of the optical energy is stored in the surrounding dielectric instead of in the metal, which leads to much smaller nonradiative losses compared with the stationary state. In addition, E_z (Figure 2G) and H_y (Figure 2H) are in-phase with a well-defined phase-front along the wavevector direction (x axis), characteristics that are similar to transverse EM waves in free space.

Compared with the stationary state, E_z of the propagating state has a much larger penetration depth into the dielectric environment, which indicates a weaker local optical field confinement.

To demonstrate that the measured dispersion in Q_{tot} is general for OLPs, we examined the optical properties of 2D arrays of Au NPs with different NP heights. Figure 3 shows that
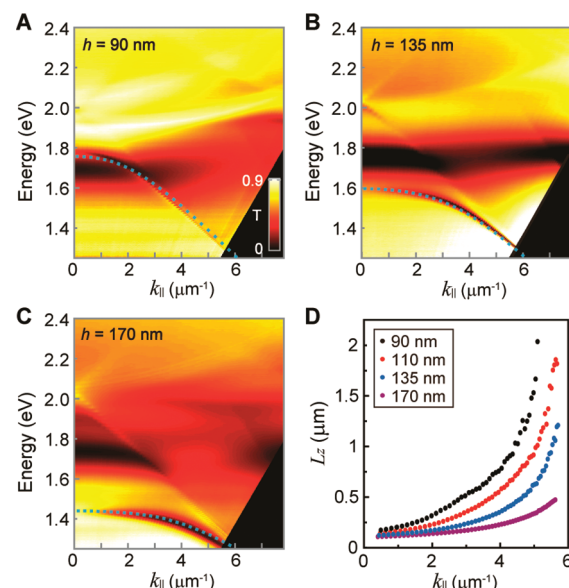
Figure 3. Dispersion properties of out-of-plane lattice plasmons significantly depend on NP height. Measured transmittance as a function of in-plane wavevector $k_{\parallel}$ and energy E in the form of dispersion diagrams for 2D Au NP arrays with NP heights of (A) 90, (B) 135, and (C) 170 nm. The dashed curves correspond to the FDTD-calculated dispersion relations of OLP. (D) Estimated decay length L_z in Au NP arrays with different NP heights confirms that OLPs exhibit tighter local field confinements at the stationary state, in agreement with FDTD-calculated E_z distribution maps in Figure 2.

OLP modes can be continuously modified by changing NP height. In contrast, other spectral features, including the dispersionless in-plane plasmon resonances associated with individual NPs and RA surface diffraction modes, are not sensitive to changes in NP height. As the height increases from h = 90 to 170 nm, the resonance energy of OLPs at the stationary state ($k_{\parallel}$ = 0) decreases from 1.78 (Figure 3A) to 1.45 eV (Figure 3C) because of the longer oscillation path-length defined by the NP height.[1] Also, the dispersion of the OLPs in NP arrays with smaller h converges with the (−1,0) RA at smaller $k_{\parallel}$. Overall, the measured dispersion relations of OLPs for NP arrays with different heights matched well with the FDTD-calculated dispersion relations (dashed curves).

As a type of surface Bloch mode, OLPs can confine EM fields to the plane of the NP array. The decay length L_z can be approximated by the first-order harmonic component bound to the surface:[19] $L_z = 1/(2*Im(k_z)); k_z^2 + (k_{\parallel} - 2\pi/a_0)^2 = (n\cdot\omega/c)^2$. Importantly, L_z can be determined from the measured E−$k_{\parallel}$ dispersion relations. Figure 3D shows that L_z increases from 150 nm at the stationary state ($k_{\parallel} \approx 0$ μm^{-1}) to 1 μm at the propagating state ($k_{\parallel} \approx 5$ μm^{-1}) for NP arrays with h = 110 nm. This result confirms the main result of the FDTD-calculated E_z distribution maps (Figure 2D,G), where the OLP exhibits a much tighter local field confinement at the stationary state. In addition, as the NP height increases, the rate of

increase in L_z with $k_\parallel$ becomes slower because the OLPs approach the propagating state at larger $k_\parallel$.

Figure 4A shows the dependence of Q_{tot}, extracted from measured optical spectra of OLPs in NP arrays with different
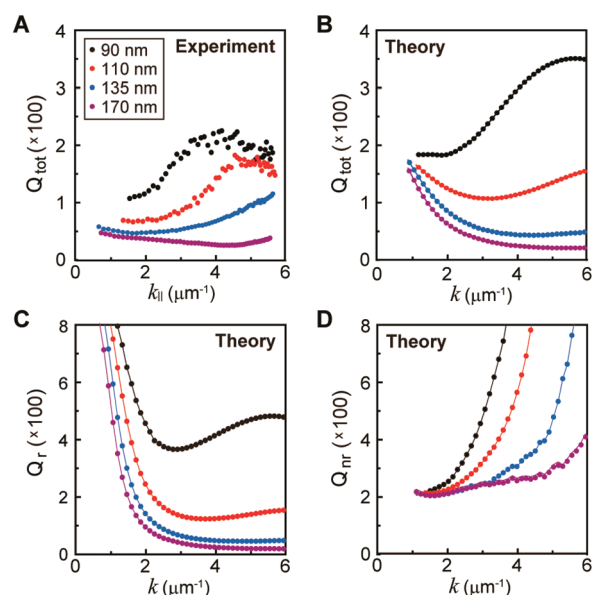
Figure 4. Q_{tot} of out-of-plane lattice plasmons is dispersive and sensitive to changes in NP height. (A) Measured total quality factors Q_{tot} and FDTD-calculated (B) Q_{tot}, (C) Q_r, and (D) Q_{nr} show that changes in NP height not only influence Q_r by determining coupling strength to the zero-order Bloch harmonic but also Q_{nr} by modifying the shape of dispersion relation of OLPs.

heights, on $k_\parallel$. Several features are apparent from these curves: (1) Over the entire $k_\parallel$ range, NP arrays of smaller heights ($h = 90$ nm, 110 nm) tend to support OLPs with larger quality factors Q_{tot} (>100); (2) at small $k_\parallel$ (<2 μm^{-1}), Q_{tot} deceases as $k_\parallel$ increases; and (3) at larger $k_\parallel$ (>2 μm^{-1}), Q_{tot} starts to increase as $k_\parallel$ increases, especially for NP arrays with smaller heights. FDTD-calculated curves of Q_{tot} (Figure 4B) qualitatively match the experimental results. Compared with good agreement for characteristics such as the plasmon wavelength, simulation and experiment of Q_{tot} will show more discrepancies because in the simulation: (1) Individual NPs are modeled as cylinders with smooth surfaces, whereas fabricated NPs have some level of surface roughness and are not perfect cylinders. This difference in geometry will affect scattering loss. (2) The dielectric constants used are those measured from Au thin films;[30] however, Au NPs may have a different imaginary part because the damping of conduction electrons is sensitive to electron scattering, which depends on crystallinity, grain size and the surface area-to-volume ratio of the metal.[31]

Using FDTD calculations, we decomposed Q_{tot} into Q_r (Figure 4C) and Q_{nr} (Figure 4D) to study how NP height affects the radiative and nonradiative depletion processes. Figure 4C shows that Q_r of OLPs is extremely large (>800) at small k (<1.5 μm^{-1}) for NP arrays with different heights and that Q_r decreases with k as the NP height increases. These trends can be explained within the framework of surface Bloch modes. Because the leaky zero-order Bloch harmonic has the same dispersion relation as free space light, the amplitude of E_{0z} for the zero-order harmonic can be expressed as $|E_{0z}| = |E_0| \cdot |k/$ $(n \cdot \omega/c)|$, where E_0 corresponds to the total electric field for zero-order harmonic. As k approaches 0, the coupling between the zero-order harmonic and high-order harmonics becomes very weak because E_{0z} of the zero-order harmonic also approaches 0. Because the coupling strength of the zero-order harmonic and higher order harmonics in a grating depends on the amplitude of the periodic modulation,[32] the plasmon energy stored in the evanescent modes is depleted faster by radiative decay in NPs with larger heights. Figure 4D shows that as the NP height increases, the increase in Q_{nr} with k becomes less significant. The reason is that NP arrays with larger NP heights support OLPs with stationary character over a broader k range before converging with the $(-1,0)$ RA at high k. Therefore, changes in the NP height not only affect Q_r by dictating the coupling strength to the leaky zero-order harmonic but also affect Q_{nr} by modifying the shape of the dispersion relation of OLPs.

In summary, our work has reported a new type of delocalized lattice plasmon in periodic NP arrays. We have clarified the dispersion effects on both far-field and near-field optical properties of delocalized OLPs. We discovered that both radiative and nonradiative processes for energy dissipation are strongly related to the dispersion relation of OLPs, which can be tailored by controlling the NP height. For applications based on delocalized lattice plasmons, therefore, dispersion effects need to be considered to achieve simultaneously narrow resonance linewidths and high local field confinements. We have shown that lattice plasmons combine the advantages of LSPs in isolated NPs (high field confinements) and SPPs on continuous metal surfaces (dispersion tunability); these plasmon excitations offer opportunities from biological and chemical sensing to surface enhanced spectroscopies to photocatalysis.

■ **AUTHOR INFORMATION**

Corresponding Author
*E-mail: todom@northwestern.edu.

Notes
The authors declare no competing financial interest.

■ **REFERENCES**

(1) Maier, S. A. *Plasmonics: Fundamentals and Applications.* Springer: New York, 2007.
(2) Barnes, W. L.; Dereux, A.; Ebbesen, T. W. Surface Plasmon Subwavelength Optics. *Nature* **2003**, *424*, 824−830.
(3) Noginov, M. A.; Zhu, G.; Belgrave, A. M.; Bakker, R.; Shalaev, V. M.; Narimanov, E. E.; Stout, S.; Herz, E.; Suteewong, T.; Wiesner, U.

1384

dx.doi.org/10.1021/jz300318v | *J. Phys. Chem. Lett.* 2012, 3, 1381−1385

Demonstration of a Spaser-Based Nanolaser. *Nature* **2009**, *460*, 1110–1168.

(4) Oulton, R. F.; Sorger, V. J.; Zentgraf, T.; Ma, R. M.; Gladden, C.; Dai, L.; Bartal, G.; Zhang, X. Plasmon Lasers at Deep Subwavelength Scale. *Nature* **2009**, *461*, 629–632.

(5) Liu, M.; Yin, X. B.; Ulin-Avila, E.; Geng, B. S.; Zentgraf, T.; Ju, L.; Wang, F.; Zhang, X. A Graphene-Based Broadband Optical Modulator. *Nature* **2011**, *474*, 64–67.

(6) Nie, S. M.; Emery, S. R. Probing Single Molecules and Single Nanoparticles by Surface-Enhanced Raman Scattering. *Science* **1997**, *275*, 1102–1106.

(7) Mühlschlegel, P.; Eisler, H.-J.; Martin, O. J. F.; Hecht, B.; Pohl, D. W. Resonant Optical Antennas. *Science* **2005**, *308*, 1607–1609.

(8) Cai, W. S.; Vasudev, A. P.; Brongersma, M. L. Electrically Controlled Nonlinear Generation of Light with Plasmonics. *Science* **2011**, *333*, 1720–1723.

(9) Klar, T.; Perner, M.; Grosse, S.; von Plessen, G.; Spirkl, W.; Feldmann, J. Surface-Plasmon Resonances in Single Metallic Nanoparticles. *Phys. Rev. Lett.* **1998**, *80*, 4249–4252.

(10) Voisin, C.; Del Fatti, N.; Christofilos, D.; Vallee, F. Ultrafast Electron Dynamics and Optical Nonlinearities in Metal Nanoparticles. *J. Phys. Chem. B* **2001**, *105*, 2264–2280.

(11) Wang, F.; Shen, Y. R. General Properties of Local Plasmons in Metal Nanostructures. *Phys. Rev. Lett.* **2006**, *97*, 206806.

(12) Christ, A.; Ekinci, Y.; Solak, H. H.; Gippius, N. A.; Tikhodeev, S. G.; Martin, O. J. F. Controlling the Fano Interference in a Plasmonic Lattice. *Phys. Rev. B* **2007**, *76*, 201405.

(13) Fedotov, V. A.; Rose, M.; Prosvirnin, S. L.; Papasimakis, N.; Zheludev, N. I. Sharp Trapped-Mode Resonances in Planar Metamaterials with a Broken Structural Symmetry. *Phys. Rev. Lett.* **2007**, *99*, 147401.

(14) Hao, F.; Sonnefraud, Y.; Van Dorpe, P.; Maier, S. A.; Halas, N. J.; Nordlander, P. Symmetry Breaking in Plasmonic Nanocavities: Subradiant LSPR Sensing and a Tunable Fano Resonance. *Nano Lett.* **2008**, *8*, 3983–3988.

(15) Zou, S. L.; Janel, N.; Schatz, G. C. Silver Nanoparticle Array Structures That Produce Remarkably Narrow Plasmon Lineshapes. *J. Chem. Phys.* **2004**, *120*, 10871–10875.

(16) Auguie, B.; Barnes, W. L. Collective Resonances in Gold Nanoparticle Arrays. *Phys. Rev. Lett.* **2008**, *101*, 143902.

(17) Chu, Y. Z.; Schonbrun, E.; Yang, T.; Crozier, K. B. Experimental Observation of Narrow Surface Plasmon Resonances in Gold Nanoparticle Arrays. *Appl. Phys. Lett.* **2008**, *93*, 181108.

(18) Kravets, V. G.; Schedin, F.; Grigorenko, A. N. Extremely Narrow Plasmon Resonances Based on Diffraction Coupling of Localized Plasmons in Arrays of Metallic Nanoparticles. *Phys. Rev. Lett.* **2008**, *101*, 087403.

(19) Vecchi, G.; Giannini, V.; Rivas, J. G. Surface Modes in Plasmonic Crystals Induced by Diffractive Coupling of Nanoantennas. *Phys. Rev. B* **2009**, *80*, 201401.

(20) Zhou, W.; Odom, T. W. Tunable Subradiant Lattice Plasmons by out-of-Plane Dipolar Interactions. *Nat. Nanotechnol.* **2011**, *6*, 423–427.

(21) Kocabas, A.; Senlik, S. S.; Aydinli, A. Slowing Down Surface Plasmons on a Moire Surface. *Phys. Rev. Lett.* **2009**, *102*, 063901.

(22) Ochiai, T.; Sakoda, K. Dispersion Relation and Optical Transmittance of a Hexagonal Photonic Crystal Slab. *Phys. Rev. B* **2001**, *63*, 125107.

(23) Fan, S. H.; Joannopoulos, J. D. Analysis of Guided Resonances in Photonic Crystal Slabs. *Phys. Rev. B* **2002**, *65*, 235112.

(24) Loncar, M.; Nedeljkovic, D.; Pearsall, T. P.; Vuckovic, J.; Scherer, A.; Kuchinsky, S.; Allan, D. C. Experimental and Theoretical Confirmation of Bloch-Mode Light Propagation in Planar Photonic Crystal Waveguides. *Appl. Phys. Lett.* **2002**, *80*, 1689–1691.

(25) Ryu, H. Y.; Notomi, M.; Lee, Y. H. Finite-Difference Time-Domain Investigation of Band-Edge Resonant Modes in Finite-Size Two-Dimensional Photonic Crystal Slab. *Phys. Rev. B* **2003**, *68*, 045209.

(26) Liu, M. Z.; Lee, T. W.; Gray, S. K.; Guyot-Sionnest, P.; Pelton, M. Excitation of Dark Plasmons in Metal Nanoparticles by a Localized Emitter. *Phys. Rev. Lett.* **2009**, *102*, 107401.

(27) Nuzzo, R. G.; Stewart, M. E.; Mack, N. H.; Malyarchuk, V.; Soares, J. A. N. T.; Lee, T. W.; Gray, S. K.; Rogers, J. A. Quantitative Multispectral Biosensing and 1D Imaging Using Quasi-3D Plasmonic Crystals. *Proc. Natl. Acad. Sci. U.S.A.* **2006**, *103*, 17143–17148.

(28) Engelen, R. J. P.; Mori, D.; Baba, T.; Kuipers, L. Subwavelength Structure of the Evanescent Field of an Optical Bloch Wave. *Phys. Rev. Lett.* **2009**, *102*, 023902.

(29) Zhang, X.; Yang, X. D.; Ishikawa, A.; Yin, X. B. Hybrid Photonic - Plasmonic Crystal Nanocavities. *ACS Nano* **2011**, *5*, 2831–2838.

(30) Johnson, P. B.; Christy, R. W. Optical-Constants of Noble-Metals. *Phys. Rev. B* **1972**, *6*, 4370–4379.

(31) Link, S.; El-Sayed, M. A. Spectral Properties and Relaxation Dynamics of Surface Plasmon Electronic Oscillations in Gold and Silver Nanodots and Nanorods. *J. Phys. Chem. B* **1999**, *103*, 8410–8426.

(32) Zaidi, S. H.; Yousaf, M.; Brueck, S. R. J. Grating Coupling to Surface Plasma-Waves 0.1. 1st-Order Coupling. *J. Opt. Soc. Am. B* **1991**, *8*, 770–779.